DDX5 helicase resolves G-quadruplex and is involved in *MYC* gene transcriptional activation

Guanhui Wu[a], Zheng Xing[b], Elizabeth J. Tran[b,c,1], and Danzhou Yang[a,c,d,1]

[a]Department of Medicinal Chemistry and Molecular Pharmacology, College of Pharmacy, Purdue University, West Lafayette, IN 47907; [b]Department of Biochemistry, Purdue University, West Lafayette, IN 47907; [c]Purdue University Center for Cancer Research, Purdue University, West Lafayette, IN 47906; and [d]Purdue Institute for Drug Discovery, Purdue University, West Lafayette, IN 47907

Edited by Thomas R. Cech, University of Colorado, Boulder, CO, and approved August 23, 2019 (received for review May 26, 2019)

G-quadruplexes (G4) are noncanonical secondary structures formed in guanine-rich DNA and RNA sequences. *MYC*, one of the most critical oncogenes, forms a DNA G4 in its proximal promoter region (MycG4) that functions as a transcriptional silencer. However, MycG4 is highly stable in vitro and its regulatory role would require active unfolding. Here we report that DDX5, one of the founding members of the DEAD-box RNA helicase family, is extremely proficient at unfolding MycG4-DNA. Our results show that DDX5 is a highly active G4-resolvase that does not require a single-stranded overhang and that ATP hydrolysis is not directly coupled to G4-unfolding of DDX5. The chromatin binding sites of DDX5 are G-rich sequences. In cancer cells, DDX5 is enriched at the *MYC* promoter and activates *MYC* transcription. The DDX5 interaction with the *MYC* promoter and DDX5-mediated *MYC* activation is inhibited by G4-interactive small molecules. Our results uncover a function of DDX5 in resolving DNA and RNA G4s and suggest a molecular target to suppress *MYC* for cancer intervention.

G-quadruplex | MYC | DDX5 | cancer drug target | G4-helicase

G-quadruplexes (G4s) are 4-stranded, noncanonical secondary structures formed in guanine-rich DNA and RNA sequences (1, 2). G4 structures are built upon stacked square-planar G-tetrads connected with Hoogsteen hydrogen-bonds and stabilized by monovalent cations, such as K^+ or Na^+ (3). DNA G4s have recently been found to be involved in a number of critical cellular processes, including gene transcription, replication, and genome instability (4–7). In particular, *MYC*, one of the most commonly deregulated genes in human cancers, has a G4 DNA motif in its proximal G/C-rich promoter region, known as the nuclease hypersensitive element III_1 (NHE III_1; also known as the CT element) (Fig. 1*A*), that functions as a transcriptional silencer element (4, 8–11). Recently, DNA G4s have been visualized in chromosomes in human cells using a G4-specific antibody (12), revealing enrichment of these structures in regulatory regions of chromatin, particularly the *MYC* promoter (13). Transcriptional regulation of *MYC* expression is complex, with P1 and P2 being the predominant promoters (14, 15). The NHE III_1 element is upstream of the P1 and P2 promoters and is an important *cis*-element for transcriptional regulation of *MYC* (9, 16) (Fig. 1*A*). When the *MYC* gene is not actively transcribed, inherent supercoiling generally does not make MycG4 to form in the double-stranded promoter region (17). However, in highly transcribed cells, the transcription machinery generates dynamic, negative supercoiling behind the moving machinery (18–20). This dynamic, transcription-coupled negative supercoiling can be transmitted to the NHE III_1 region, where it promotes melting of genomic DNA to the intermediate single-stranded forms that can spontaneously form the metastable stable G4 structures (21–24). The formation of G4s in the *MYC* promoter inhibits *MYC* transcription by preventing the binding of double-stranded (Sp1) or single-stranded (CNBP and hnRNP K) transcriptional factors (8, 25). Compounds that bind and stabilize this G4 have been shown to reduce *MYC* expression and are antitumorigenic (4, 8, 26). We previously determined the molecular structure of the major G4 formed in the *MYC* promoter NHE III_1 G-rich strand (Pu28) (Fig. 1*A*) in physiologically relevant K^+ solution, revealing a parallel-stranded structure (27) (MycG4) (Fig. 1*B*). The MycG4 structure is very stable under physiologically relevant salt conditions with a melting temperature over 85 °C in 100 mM K^+ solution (28–30). Therefore, regulation of *MYC* expression would require active unfolding of the MycG4 G4 structure. Such a resolvase, however, has yet to be discovered.

DEAD-box (DDX) proteins define the largest family of double-stranded RNA (dsRNA) helicases, which contain 12 conserved sequence motifs, including the eponymous DEAD motif (Asp-Glu-Ala-Asp, or D-E-A-D) (31). The DEAD-box helicases are unique among helicase families, in that they are nondirectional and nonprocessive. The human DEAD-box protein 5 (DDX5), also named p68, is one of the founding members of the DEAD-box RNA helicase family and is implicated in a number of critical cellular processes, including cell proliferation and organ development (32–35). While its level is low in normal cells, DDX5 is overexpressed in a number of major human cancers—including colon, lung, breast, and prostate—and is shown to promote tumorigenesis, tumor progression, and cellular transformation (36–41). DDX5 has been suggested to be a transcriptional regulator (36, 42, 43). The DDX5 yeast ortholog Dbp2 has been shown to directly associate with transcriptionally active chromatin (44, 45). Intriguingly, DDX5 has been shown to activate *MYC* expression in multiple solid tumors by an unknown mechanism (38, 39, 46). However, the mechanism of transcriptional regulation by DDX5 is poorly understood, as the RNA helicase

Significance

G-quadruplexes (G4) are 4-stranded nucleic acid secondary structures. *MYC* is a critical oncogene with a G4 in its promoter (MycG4), which acts as a transcription silencer. MycG4 is very stable and the pathological activation of *MYC* in cancers requires its active unfolding. We reveal herein that DDX5, a founding member of the DEAD-box RNA helicase family, can unfold DNA G4s. The unfolding mechanism of DDX5 is distinct from previously characterized G4 helicases. Importantly, DDX5 activates *MYC* gene transcription by proficiently unfolding the promoter MycG4. DDX5 is overexpressed in cancers and the DDX5–MycG4 interaction can be inhibited by small molecules to downregulate *MYC*. Therefore, our results suggest a new molecular target to suppress *MYC* for cancer intervention.

Author contributions: G.W., E.J.T., and D.Y. designed research; G.W. and Z.X. performed research; G.W., Z.X., E.J.T., and D.Y. analyzed data; and G.W. and D.Y. wrote the paper.

The authors declare no conflict of interest.

This article is a PNAS Direct Submission.

[1]To whom correspondence may be addressed. Email: ejtran@purdue.edu or yangdz@purdue.edu.

This article contains supporting information online at www.pnas.org/lookup/suppl/doi:10.1073/pnas.1909047116/-/DCSupplemental.

First Published September 23, 2019.

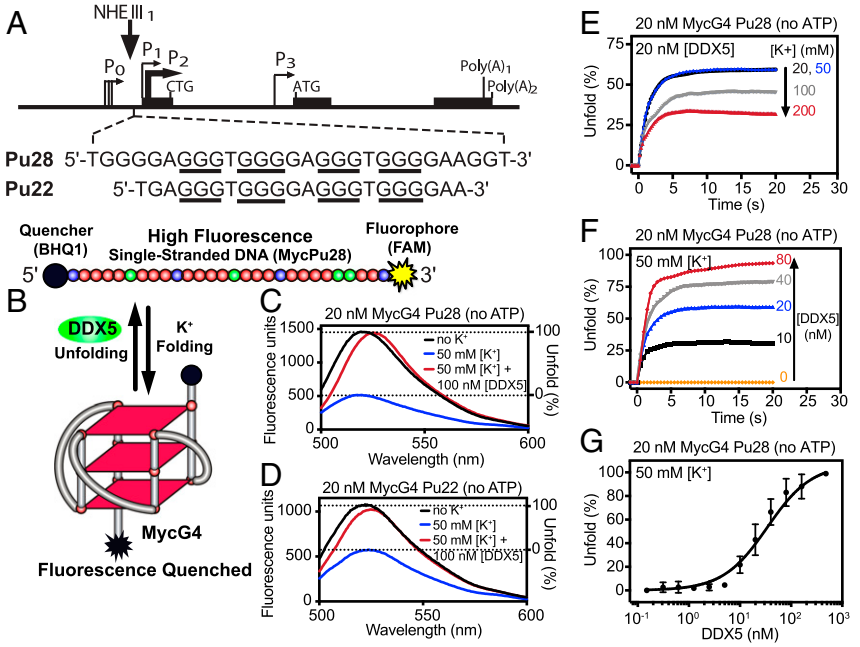

Fig. 1. DDX5 actively unfolds MycG4 and is a potent G4 unfolding protein. (*A*) The *MYC* promoter structure with the G4-forming region NHE III_1 sequence Pu28 is shown. The truncated Pu22 sequence that forms the major MycG4 is also shown. (*B*) A molecular beacon MycG4 FRET probe was designed for helicase unfolding assays using the MycG4 Pu28 and MycG4 Pu22 sequences. Each oligo was labeled with the fluorophore 6-FAM on the 3′ end and quencher BHQ-1 on the 5′ end. (*C* and *D*) MycG4 unfolding by DDX5 in MycG4 Pu28 (*C*) and MycG4 Pu22 (*D*). Percent of MycG4 unfolding was calculated as $100 \times \Delta F/\Delta F_{max}$, where ΔF_{max} = (black line – blue line), the difference of fluorescence between the unfolded probe (black line) in 0 mM K^+ and the folded probe (blue line) in 50 mM K^+ solution (50 mM pH 7.4 Tris-acetate, 20 nM MycG4 Pu28 or MycG4 Pu22, 2.5 mM $MgCl_2$, no ATP), and ΔF = (red line – blue line), the fluorescence change after adding DDX5 (red line) from the folded probe (blue line). (*E*) Time course analysis of 20 nM MycG4 unfolding by 20 nM DDX5 at various concentrations of K^+ (20, 50, 100, and 200 mM) (no ATP). For relative binding of DDX5 to MycG4 at different concentrations of K^+, see *SI Appendix*, Fig. S3*A*. (*F*) Time-course analysis of 20 nM MycG4 unfolding at various concentrations of DDX5 (0, 10, 20, 40, and 80 nM) in 50 mM K^+ (no ATP) showing DDX5 unfolds MycG4 in a dose-dependent manner. MycG4 Pu28 FRET probe was used as the substrate. (*G*) The observed Michaelis constant (K_m) for DDX5-mediated G4 unfolding was 32 ± 8 nM of DDX5 (50 mM K^+, no ATP). Unfolding reactions were incubated for 5 min before taking fluorescence measurements. n = 3 independent measurements. Error bars represent mean ± SD.

activity of DDX5 does not seem to be required for transcriptional regulation in many cases (36, 43).

Here we report that DDX5 is a highly active DNA and RNA G4 resolvase that does not require a single-stranded overhang. ATP hydrolysis is shown not to be directly coupled to the DDX5 G4-unfolding. DDX5 proficiently unfolds the *MYC* promoter DNA G4 and activates *MYC* expression in human cancer cells in a G4-dependent manner. Furthermore, the DDX5 unfolding of MycG4 and DDX5-induced *MYC* activation are inhibited by G4-stabilizing small molecules. Thus, the DDX5–MycG4 interaction represents a potential future target for *MYC* down-regulation for cancer intervention.

Results

Characterization of DDX5 as a Proficient G4 Resolvase. We first investigated the G4-unfolding activities of DDX5. We designed a fluorescence resonance energy transfer (FRET) probe using the full-length *MYC* promoter G4 DNA (MycG4-Pu28) (Fig. 1*A* and *SI Appendix*, Table S1), which is labeled with 6-fluorescein (6-FAM) on the 3′-end and black hole-1 quencher (BHQ-1) on the 5′-end (Fig. 1*B*). The stable formation of G4s requires the presence of K^+ or Na^+ cations, with a preference for K^+ (Fig. 1*B*). In the absence of K^+, the MycG4-Pu28 existed in the single-stranded form with the 2 ends far apart, as evidenced by high FAM-fluorescence (Fig. 1 *B*, *Upper*, and Fig. 1*C*, black line). In the presence of 50 mM K^+, DNA G4 is formed and FAM-fluorescence was quenched (Fig. 1*C*, blue line). Upon addition of DDX5 (*SI Appendix*, Fig. S1) to MycG4-Pu28 DNA in the K^+ solution, the FAM-fluorescence was dramatically increased (Fig. 1*C*, red line) to the same level of unfolded Pu28 in the absence of K^+ (Fig. 1*C*, black line), indicating that MycG4 is unfolded to the single-stranded form by DDX5.

A unique feature of DEAD-box helicases is that they separate strands locally rather than in a translocation-based manner, therefore their dsRNA unwinding activity does not require an extended flanking tail (31, 47). All active G4 helicases reported to date require a long single-stranded tail at either the 3′- or 5′-end for loading and subsequent G4-unfolding (34). To test whether the extended tail is needed for G4-unfolding by DDX5, we first prepared a truncated MycG4 FRET probe, MycG4-Pu22 (27), which contains the 4 guanine-runs with minimal flanking capping segments that are required to form the well-defined major G4 conformation in the full-length MycG4-Pu28. Upon addition of DDX5, the FAM-fluorescence was dramatically increased (Fig. 1*D*), indicative of MycG4-Pu22 unfolding by DDX5, as observed for Pu28 (Fig. 1*C*). We then prepared MycG4-Pu16 that contains only the core G4-forming sequence without any flanking segments and found the same G4-unfolding activity of DDX5 (*SI Appendix*, Fig. S2). These results demonstrate that DDX5 can load on and unfold the MycG4 without extended flanking tails.

We next examined the effect of K^+ because it can stabilize G4 structures (28). Using equimolar concentrations of DDX5 and DNA (20 nM), the MycG4 unfolding activity of DDX5 was similar in 20 mM and 50 mM K^+ concentrations (50%). Increasing the K^+ concentration above 50 mM reduced the unfolding activity of DDX5 (Fig. 1*E*). Because DDX5 showed high unfolding amplitudes up to 50 mM K^+, this potassium concentration was used in most FRET assays.

To investigate the unfolding activity of DDX5, we carried out time-course analyses of G4-unfolding by DDX5 using the FRET assays. The results revealed that the MycG4 structure was rapidly unfolded by DDX5, with a half-time of a few seconds (Fig. 1 *E* and *F*). In addition, DDX5 appeared to unfold the MycG4 Pu28 in a dose-dependent manner (Fig. 1*F*); DDX5 unfolds about 50% of MycG4 DNA at equimolar concentration of DNA (20 nM). The observed Michaelis constant (K_m) of unfolding of MycG4 Pu28 DNA was 32 ± 8 nM of DDX5 (Fig. 1*G*).

Taken together, our results demonstrate that DDX5 proficiently unfolds G4 DNA without a requirement for single-stranded DNA (ssDNA) tail, representing a distinct mechanism among known G4 helicases to date.

G4s Are Preferred Substrates of DDX5 In Vitro and In Vivo. We next measured the G4 binding activity of DDX5. Utilizing biotinylated DNA immobilized to streptavidin-coated plates in an ELISA, we measured the direct binding of DDX5 to various DNA substrates in 100 mM K^+ solution (Fig. 2*A*). DDX5 displayed a high binding affinity to MycG4 DNA, markedly greater than to ssDNA (Fig. 2*A*). As K^+ induces (48) and stabilizes (28) the G4-formation, we tested the relative binding of DDX5 to immobilized unannealed MycG4 DNA in ELISA in the presence of increasing concentrations of K^+. These results showed that K^+ enhances the DDX5 binding of MycG4 DNA, with maximal binding at 50 mM K^+ (*SI Appendix*, Fig. S3*A*). This observation may explain the similar G4-unfolding activity of DDX5 in 20 mM and 50 mM K^+ concentrations (Fig. 1*E*). The dissociation constant (K_d) of DDX5 binding to MycG4 DNA was determined to be 13 ± 1 nM using fluorescence anisotropy (*SI Appendix*, Fig. S3*B*). Additionally, DDX5 showed a preference to the G-rich sequence over other non-G-rich sequences in the presence of K^+ (*SI Appendix*, Fig. S3*C*).

To test whether DDX5 binds to RNA G4 structures, or other double- or single-stranded DNA and RNA conformations, we performed ELISA competition experiments using immobilized MycG4 DNA. The binding of DDX5 to immobilized MycG4 DNA was significantly inhibited by both DNA and RNA G4 structures (Fig. 2*B*), but not by other DNA or RNA conformations, such as dsRNA, RNA hairpin, ssRNA, and dsDNA, DNA hairpin, and ssDNA (Fig. 2*C*). Importantly, the MycG4 DNA and MycG4 RNA showed the same inhibitory activity of DDX5 binding to immobilized MycG4 DNA (Fig. 2*B*), suggesting DDX5 recognizes the G4 conformation through a structure-based mechanism. The binding of DDX5 to MycG4 was confirmed by EMSA (*SI Appendix*, Fig. S3*D*). Addition of DDX5 to the MycG4 DNA caused significant changes to the migration of the unbound probe. We attribute the shift of the unbound probe to the binding and unwinding of DDX5, as well as gradual dissociation of the unfolded DNA from the DDX5-complex during the gel running process, which has been observed in other protein–DNA systems (49).

We then investigated the DDX5's preferred chromatin-binding sites reported in vivo. We analyzed publicly available DDX5 chromatin immunoprecipitation-sequencing (ChIP-seq) data (50), which was obtained from HeLa S3 cells that have high expression levels of both DDX5 and Myc (*SI Appendix*, Fig. S4). We found that most of the top 15 DDX5-binding motifs identified by MEME (motif-based sequence analysis tools) (51) are G-rich sequences (*SI Appendix*, Fig. S5*A*), suggesting G4 structures are one of the preferred substrates for DDX5 in human chromatin.

ATP Hydrolysis Is Not Directly Coupled to G4-Unfolding by DDX5. Unexpectedly, our results showed that the unfolding activities of DDX5 on the MycG4 structure occurred in the absence of ATP (Fig. 1). DDX5's binding and unwinding activity of dsRNA is ATP-dependent and saturated at 2 mM ATP (52). To confirm

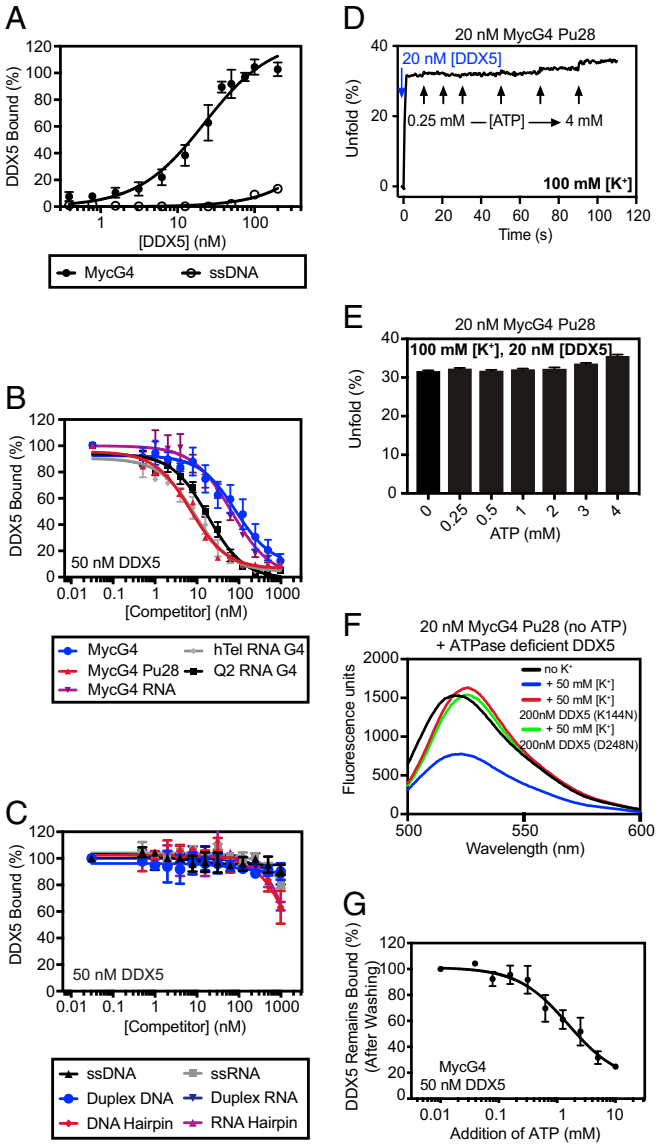

Fig. 2. DDX5 preferentially recognizes and unfolds G4 structures in an ATP-independent manner. (*A*) Binding determined by ELISA in 100 mM K^+ showing that DDX5 has a high affinity for MycG4 structure ($K_d = 22 \pm 2$ nM). K_d was calculated using the 1-site specific binding equation. $n = 3$ to 6 independent measurements. Error bars represent mean ± SD. (*B* and *C*) Competition binding ELISA experiments with the immobilized MycG4 DNA in showing DDX5 preferentially recognizes G4 structures. DDX5 was coincubated with increasing concentrations of either G4-forming oligonucleotides (MycG4 Pu28, MycG4, MycG4 RNA, TERRA RNA G4, or Q2 RNA G4) (*B*) or non-G4–forming oligonucleotides (ssDNA, ssRNA, DNA hairpin, RNA hairpin, dsDNA, or dsRNA) (*C*). Data were fitted with a 1-site competition binding equation. $n = 4$ to 6 independent measurements. Error bars represent mean ± SD. (*D* and *E*) Time-course analysis of 20 nM MycG4 FRET unfolding in 100 mM K^+ showing that the unfolding of MycG4 by DDX5 is slightly enhanced by the addition of ATP (*D*). Black arrows from left to right correspond to total concentrations of ATP in the solution (0.25, 0.5, 1, 2, 3, and 4 mM). The blue arrows correspond to the concentration of DDX5 in the solution (20 nM). The percentages of 20 nM MycG4 unfolding by 20 nM DDX5 in 100 mM K^+ at different ATP concentrations are as follows: 32%, 32%, 32%, 32%, 32%, 34%, and 35%, from left to right (*E*). (*F*) G4 unfolding FRET assay showing the ATPase-deficient DDX5 mutant proteins K144N and D248N are able to unfold MycG4 structures. The mutant DDX5 protein K144N cannot bind ATP, while D248N can bind but not hydrolyze ATP. (*G*) ELISA experiments showing the addition of ATP into DDX5/MycG4 complex decreases the population of DDX5 bound to MycG4 after washing steps. Different concentrations of ATP were added to wells containing the DDX5 complex with immobilized MycG4. After incubation, ATP and transiently released DDX5 were washed away prior to the addition of antibodies. $n = 3$ biologically independent samples. Error bars represent mean ± SEM.

that our observations were not caused by ATP contamination of purified DDX5, hexokinase and glucose were added to purified protein prior to the assessment of its G4 unfolding activity. Hexokinase phosphorylates glucose using ATP and has been used previously to deplete copurifying ATP from helicase protein preparations (53). No significant difference in MycG4 unwinding activity was observed with or without pretreatment of hexokinase (*SI Appendix*, Fig. S6), indicating our observations were not because of ATP contamination. To further investigate the effect of ATP, we titrated ATP into the unfolding reaction up to 4 mM. Our results showed that the addition of ATP does not appreciably alter the MycG4 unfolding activity of DDX5 (Fig. 2 *D* and *E*).

To confirm the ATP-independence of DDX5 G4-unfolding, we examined MycG4 unfolding using 2 ATPase-deficient mutant DDX5 helicases, mutant K144N and D248N (Fig. 2*F*). The mutant DDX5 protein K144N cannot bind ATP, while D248N can bind but cannot hydrolyze ATP (54). In contrast to dsRNA unwinding, which is ATP-dependent, our results showed that both of the DDX5 mutant proteins were able to unfold MycG4. This suggests that DDX5 utilizes a mechanism for unwinding G4 that is distinct from dsRNA unwinding.

We further examined the effects of ATP on the binding of DDX5 to MycG4-DNA. Interestingly, the addition of ATP to the preformed complex of DDX5 and immobilized MycG4-DNA in ELISA experiments followed by washing steps significantly reduced the amount of DDX5 protein bound to immobilized MycG4-DNA (Fig. 2*G*). Since the addition of ATP did not change DDX5 unfolding activity in the FRET assays (Fig. 2 *D* and *E*), which didn't contain washing steps, this result suggests that ATP is likely required for release of unfolded G4 from DDX5. Collectively, these data suggest that the ATP hydrolysis is not directly coupled to G4-unfolding by DDX5.

Conformational Change of MycG4 DNA Induced by DDX5. To investigate the conformational change of the MycG4-DNA induced by DDX5, we carried out dimethylsulphate (DMS) footprinting experiments in which exposed N7s of guanine nucleotides are methylated by DMS, cleaved by subsequent piperidine treatment, and then visualized on a sequencing gel (55). G-tetrad (Fig. 3*A*) formation (4) and protein/nucleic acid interactions (55) have been shown to protect the N7s of guanines against DMS methylation, while protein-induced DNA/RNA conformational changes can alter the DMS methylation-induced cleavage pattern (55–57). In the presence of K^+, 4 consecutive G-runs (R2 to R5) of Pu28 displayed a clear protection pattern against DMS methylation-induced cleavage (Fig. 3*B*, lane 2), indicating the formation of MycG4 in the Pu28 sequence (Fig. 1*B*) (4). Addition of DDX5 to the Pu28 DNA enhanced DMS methylation-induced cleavage (Fig. 3*B*, lane 3) as compared to free Pu28 (Fig. 3*B*, lane 2 and autoradiogram densitometric scans). In the presence of DDX5, guanines in the G-run R5 showed significantly greater cleavage, while both R3 and R4 G-runs showed higher cleavage, indicating N7s of guanines in G-runs R3, R4, and R5 were more exposed to DMS methylation. This result demonstrates that the intramolecular G4 structure was disrupted by DDX5. Interestingly, R2, R3, and R4 were still partially protected from DMS-methylation–induced cleavage (Fig. 3*B*, compare lane 1 and lane 3), suggesting association of DDX5 with the unfolded MycG4 DNA.

We also performed CD spectroscopy measurements to analyze the conformational change of MycG4 induced by DDX5. The MycG4-Pu28 DNA forms a parallel-type G4 structure in K^+ solution, as shown by a characteristic CD maximum at 260 nm (28) (Fig. 3*C*). DDX5 protein does not have any signal at 260 nm (Fig. 3*D*). Upon addition of DDX5 to MycG4 Pu28 DNA, the CD intensity at 260 nm decreased as the concentration of DDX5 increased (Fig. 3*C*), indicating the disruption of G4 structure by DDX5.

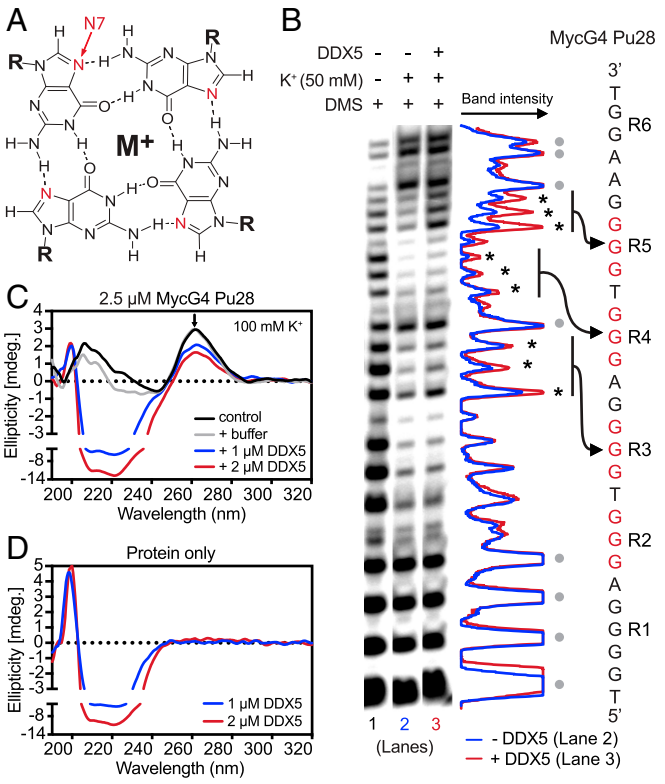

Fig. 3. DMS footprinting and CD spectroscopy showing the conformation change of MycG4 induced by DDX5. (*A*) Schematic diagram showing the structure of G4. N7s of guanine nucleotides are labeled in red. M^+ represents monovalent metal cation. (*B*) DMS methylation assay of the MycG4 Pu28 showing the conformational change of Pu28 induced by DDX5. Pu28 oligonucleotides were incubated with DMS for 21 min at appropriate conditions. Autoradiogram densitometric scans are shown to the right of the gel comparing Pu28 cleavage patterns in the absence (blue; lane 2) and presence (red; lane 3) of DDX5 (500 nM). Guanines with enhanced cleavage in the presence of DDX5 are labeled with black asterisks. Guanines that are not involved in G4 formation (and therefore have very similar cleavage patterns in the absence and presence of DDX5) are labeled with gray dots. The uncropped image is shown in *SI Appendix*, Fig. S10. (*C*) CD titration spectra of MycG4 Pu28 in 100 mM K^+ solution with increasing concentrations of DDX5. MycG4 Pu28 forms a parallel G4 structure in the presence of 100 mM K^+, as indicated by characteristic maxima at near 260 nm (indicated by the arrow). Upon addition of DDX5, the CD intensity at 260 nm was significantly reduced. All measurements were using the same MycG4 Pu28 stock solution, with Pu28 oligonucleotides preannealed in the presence of 100 mM K^+. (*D*) CD spectra of DDX5 protein at different concentrations.

DDX5 Directly Interacts with the *MYC* Promoter G4-Forming Region and Activates *MYC* Expression in Tumorigenic Cells. DDX5 level is low in normal cells but is overexpressed in multiple human tumors (36, 37, 39–41, 58). In addition, DDX5 has been shown to activate *MYC* in tumors (38, 39, 46) and a positive feedback loop of DDX5 and Myc was suggested to contribute to tumorigenesis (46). As DNA G4s have been shown to form in the *MYC* promoter and negatively regulate *MYC* transcription (4, 13), we rationalized that DDX5 regulates *MYC* expression in a G4-dependent mechanism. To test this hypothesis, we first determined whether DDX5 directly interacts with the *MYC* G4-forming promoter region in vivo by ChIP experiments in MCF7 cells (Fig. 4*A*). The human breast cancer MCF7 cell line has been shown to have a high-level of DDX5 expression (46). The ChIP results showed that DDX5 directly interacts with the *MYC* promoter, as demonstrated by the enrichment of the *MYC* G4-forming promoter region in coimmunoprecipitated DNA (Fig. 4*A*). Note that this enrichment was lost after knocking down DDX5 by DDX5 small-interfering

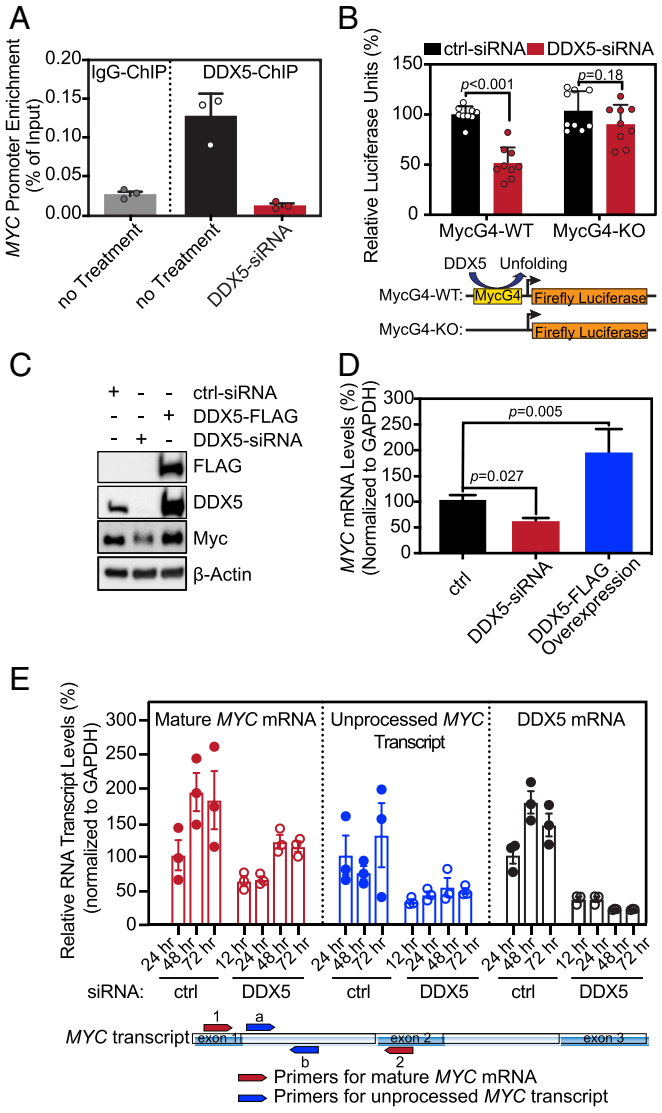

Fig. 4. DDX5 up-regulates *MYC* transcriptional activity in a G4-dependent manner. (*A*) The interaction of DDX5 with the *MYC* promoter was probed by ChIP-qPCR with or without 24-h treatment of DDX5-siRNA in MCF7 cells. DDX5 directly interacts with the *MYC* promoter at the MycG4 forming region (*Left*), whereas the MycG4 forming region cannot be detected from the immunoprecipitated DNA–protein complex after DDX5 silencing (*Center*). $n = 3$ biologically independent samples. Error bars represent mean ± SD. (*B*) Luciferase reporter assays showing that DDX5 silencing by siRNA inhibits WT, but not G4-KO, *MYC* promoter activity in MCF7 cells. Relative firefly luciferase activities produced by 2 reporters (pGL4.10-c-MYC-WT Pu43 or pGL4.10-c-MYC-KO Pu43) (59) at different conditions were normalized to the MYC-WT reporter in the presence of nontargeting control siRNA (ctrl-siRNA). *Renilla* luciferase activity produced by pRL-TK reporter was served as an internal control. $n = 9$ biologically independent samples. Error bars represent mean ± SD, *P* value was calculated by Sidak's multiple-comparisons test after 2-way ANOVA. (*C*) Representative Western blot analysis showing positively correlated expressions of Myc and DDX5 in MCF7 cells. DDX5 was either knocked down using siRNA or overexpressed using DDX5-FLAG encoding vectors in MCF7 cells. The cells were transfected with respective plasmids for 48 h before harvesting. Note: FLAG/DDX5, and Myc/β-actin were analyzed as 2 blots. The positive correlation between Myc and DDX5 expressions was further confirmed using 22Rv1 prostate cancer cell line (*SI Appendix*, Fig. S8). (*D*) *MYC* transcription is directly regulated by DDX5. DDX5 was either knocked down using siRNA or overexpressed using DDX5-FLAG encoding vectors in MCF7 cells, *MYC* mRNA levels were measured using qRT-PCR at 48 h after transfection. Error bars represent mean ± SD, *P* value was calculated by Dunnett's multiple comparisons test after 1-way ANOVA. (*E*) qRT-PCR results showing knocking-down DDX5 by siRNA decreases the levels of both unprocessed and mature *MYC* RNA transcripts at 12-, 24-, 48-, and 72-h time points. Unprocessed *MYC* RNA transcript was measured using the intron specific primers (primers a and b). Mature *MYC* mRNA levels were measured using a pair of primer flanking intron 1 (primers 1 and 2). All RNA transcript levels were measured at desired time points after the DDX5-siRNA treatments. $n = 3$ biologically independent samples. Error bars represent mean ± SEM. The same data with normalization is shown in *SI Appendix*, Fig. S7.

RNA (siRNA), indicating that the signal is not due to background. We further analyzed the published DDX5 ChIP-seq data from HeLa S3 cells (50), which showed high expression levels of both Myc and DDX5 (*SI Appendix*, Fig. S4), and found a specific enrichment of DDX5 close to the transcription start site (TSS) of the *MYC* gene, corresponding to the G4-forming region (*SI Appendix*, Fig. S5*B*).

We next employed luciferase assays using a MycG4-WT construct with the WT *MYC* promoter sequence or a MycG4-knockout (KO) construct with a MycG4-KO promoter sequence in front of the luciferase gene (59) in MCF7 cells. For the MycG4-WT construct, the promoter activities were markedly repressed by DDX5-siRNA. In contrast, a smaller effect was observed for the MycG4-KO construct (Fig. 4*B*), These results indicate that DDX5-depletion inhibits the *MYC* promoter activity when the MycG4 is present.

We then examined the Myc expression levels in MCF7 cells in response to DDX5 depletion or DDX5 overexpression. The treatments of DDX5-siRNA lowered both *MYC* protein and mRNA levels in MCF7 cells (Fig. 4 *C* and *D*). To directly assess the effect of DDX5 on *MYC* transcription, we designed 2 sets of primers (Fig. 4 *E*, *Lower*) to amplify either the unprocessed, nascent or mature *MYC* RNA transcripts by qRT-PCR at various time points following DDX5 depletion (Fig. 4*E* and *SI Appendix*, Fig. S7). Our results showed that both unprocessed and mature *MYC* transcripts were rapidly decreased within 12 h after DDX5 depletion and this effect could last up to 72 h, suggesting the direct involvement of DDX5 in the transcriptional activation of the *MYC* gene. The suppression of *MYC* expression by DDX5 depletion was also shown in a prostate carcinoma cell line 22Rv1 using 2 different DDX5-silencing shRNAs (*SI Appendix*, Fig. S8). In contrast, the overexpression of DDX5 by a DDX5-overexpression plasmid (DDX5-FLAG) promoted *MYC* expression (Fig. 4 *C* and *D*).

We then analyzed the expression levels of DDX5 and *MYC* in multiple immortalized cell lines (*SI Appendix*, Fig. S4). We found a positive correlation between the expression of *MYC* and DDX5 in tumorigenic cell lines, which showed higher DDX5 and *MYC* expression levels than nontumorigenic cell lines, suggesting that the positive correlation between *MYC* and DDX5 promotes tumorigenesis. These results indicate DDX5 directly transactivates the *MYC* transcription through the G4-forming promoter region.

DDX5-Induced MycG4-Unfolding and *MYC* Gene Activation Are Inhibited by G4-Interactive Compounds. G4 structures can be recognized and stabilized by small molecules. TMPyP4 is a G4-interactive compound, whereas its positional isomer, TMPyP2, is a poor G4-interactive compound (29, 60) (Fig. 5*A*). We examined the effects of TMPyP4 and TMPyP2 on the MycG4 unfolding activity of DDX5. Our results showed TMPyP4, but not TMPyP2, significantly inhibited the G4 unfolding activity of DDX5 (~70% inhibition) (Fig. 5*B*). We then examined the effects of TMPyP4 and TMPyP2 on the direct binding of DDX5 to the MycG4. The results showed TMPyP4 disrupted the DDX5 binding to MycG4 in a dose-dependent manner, whereas TMPyP2 did not (Fig. 5*C*). In addition, we examined Phen-DC3, another G4-interactive small molecule (Fig. 5*A*), and found it disrupted

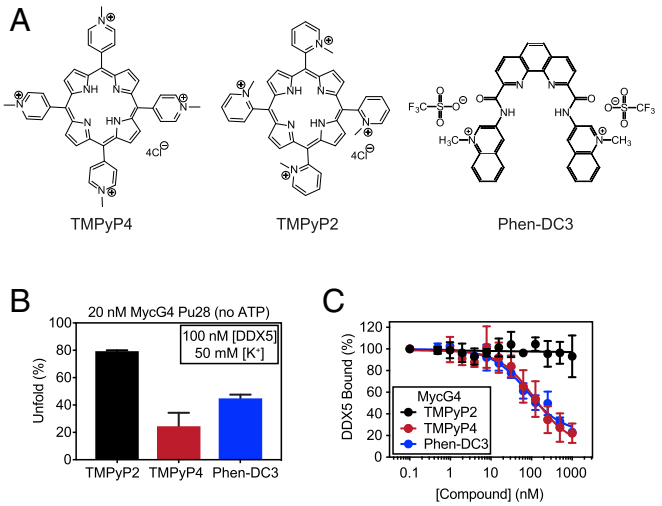

Fig. 5. G4-interactive compounds inhibit G4-binding and G4-unfolding of DDX5. (*A*) Structures of TMPyP4, TMPyP2, and Phen-DC3. (*B*) G4-interactive compound TMPyP4 (250 nM) and Phen-DC3 (250 nM), but not poor G4-interactive TMPyP2 (250 nM), inhibits MycG4 unfolding activity of DDX5. (*C*) Inhibition curves by ELISA showing that TMPyP4 and Phen-DC3, but not TMPyP2, disrupts the interaction of DDX5 to MycG4 DNA. DDX5 was coincubated with increasing concentrations of either TMPyP2, TMPyP4, or Phen-DC3 for assessment of DDX5 binding to MycG4 in ELISA. $n = 4$ to 6 independent measurements. Error bars represent mean ± SD.

the DDX5 binding to the MycG4 and inhibited MycG4 unfolding by DDX5 (Fig. 5 *B* and *C*). These data indicate that G4-interactive compounds can inhibit DDX5 G4-unfolding activity in vitro by preventing its association with G4 structure.

To investigate whether inhibition of DDX5 activity presents a mechanism of action for G4-interactive small molecule in cancer cells, we examined the effects of TMPyP4 and TMPyP2 on the DDX5 and Myc levels in MCF7 cells. We found that treatments of both TMPyP4 and TMPyP2 showed no inhibitory effects on DDX5 expression up to 48 h, whereas TMPyP4, but not TMPyP2, decreased Myc expression in both a time- and dose-dependent manner (Fig. 6*A* and *SI Appendix*, Fig. S9*A*). It is noted that while treating cells with TMPyP4 for 72 h completely knocked out the Myc expression, the DDX5 expression was also slightly repressed (Fig. 6*A*), likely reflecting previously reported positive feedback loop between MYC and DDX5 (46). Because 12 μM of TMPyP4 induced significant Myc reduction within 48 h (*SI Appendix*, Fig. S9*A*), this dosage was used in all of the subsequent cellular studies.

We further examined the effects of TMPyP4 and TMPyP2 on the Myc levels when DDX5 was overexpressed (*SI Appendix*, Fig. S9*B*). Our results showed that while the overexpression of DDX5 up-regulated the Myc expression in MCF7 cells, TMPyP4 was still able to inhibit the Myc expression, suggesting G4-interactive small molecule is able to inhibit DDX5-induced *MYC* activation in vivo.

To confirm whether the reduced Myc expression by G4-interactive compounds is related to the inhibition of the DDX5 interactions with the *MYC* G4-forming promoter, ChIP analysis was carried out in MCF7 cells with 12-h drug treatments. As a result, treating cells with TMPyP4, but not TMPyP2, led to a significant reduction (more than 50%, $P < 0.001$ versus control) of DDX5 occupancy on *MYC* promoter (Fig. 6*B*). It is important to note that DDX5 protein levels were not affected by the treatments of TMPyP4 or TMPyP2 up to 48 h (Fig. 6*A*). Taken together, these results indicate that the direct interactions of

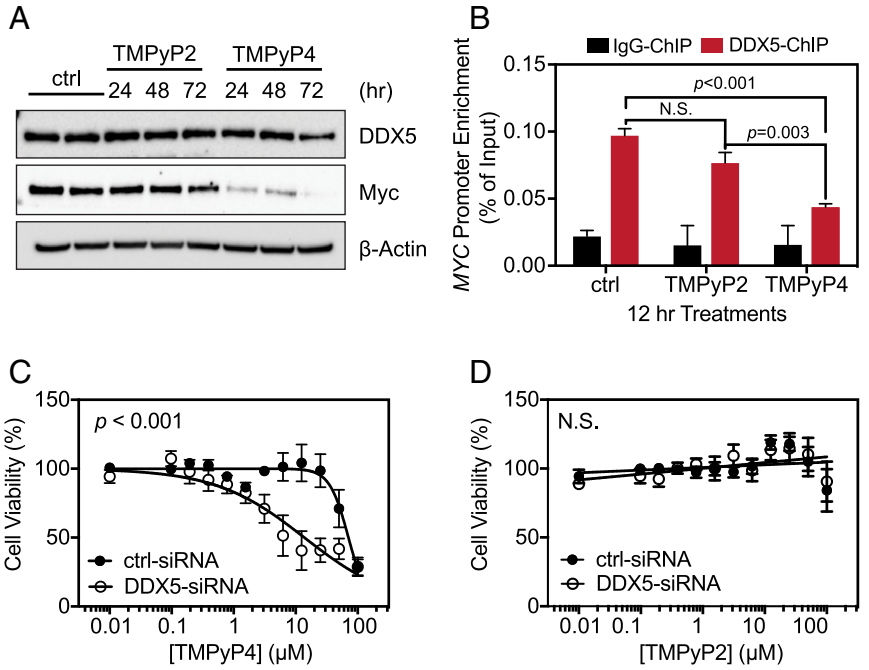

Fig. 6. G4-interactive molecules, such as TMPyP4, can disrupt transcriptional activation of DDX5 on *MYC* and lead to cancer cell death. (*A*) TMPyP4, but not TMPyP2, lowers Myc protein levels but does not affect DDX5 expression. The time of treatments with either TMPyP2 or TMPyP4 is listed at the top of the gels. (*B*) ChIP analysis of the interaction of DDX5 with the *MYC* promoter showing TMPyP4, but not TMPyP2, disrupts the interactions of DDX5 with the *MYC* promoter MycG4 forming region. The cells were either untreated (ctrl) or treated with 12 μM TMPyP2 or TMPyP4 for 12 h. For ChIP assay validation, see Fig. 4*A*. $n = 3$ biologically independent samples. Error bars represent mean ± SD *P* value was calculated by Tukey's multiple comparisons test after 2-way ANOVA. (*C* and *D*) siRNA knockdown of DDX5 increases sensitivity of MCF7 cells to the cell death caused by TMPyP4 (*C*), but not TMPyP2 (*D*). Data are mean ± SEM of 9 biologically independent samples. N.S., no significance, $P > 0.05$; *P* value for the IC_{50} comparison was calculated by extra sum-of-squares *F* test.

DDX5 with the *MYC* promoter G4 can be disrupted by G4-interactive compounds to suppress *MYC* expression.

DDX5 Inhibition and MycG4 Stabilization Lead to Synergistic Lethality in Cancer Cells. We have demonstrated that DDX5 is a highly active MycG4 unfolding resolvase that activates *MYC* transcription in a G4-dependent manner. To investigate if DDX5 and MycG4 interaction can serve as a molecular target for cancer intervention, we knocked down DDX5 prior to the addition of MycG4-stabilizing small molecule TMPyP4. We found that after DDX5 silencing, MCF7 cancer cells were more sensitive to the cell death induced by MycG4-interactive small molecule TMPyP4, but not TMPyP2 (Fig. 6 *C* and *D*). This suggests that inhibition of DDX5 and stabilization of the *MYC* promoter G4 can yield synergistic lethality in cancer cells supporting a role of DDX5 in active resolution of G4 structures in vivo. Altogether, these results demonstrate that G4-interactive ligands can target and block the DDX5 interactions with the *MYC* promoter G4, thereby disrupt transcriptional activation of DDX5 on *MYC* and lead to *MYC* down-regulation and cancer cell death.

ChIP Analysis of DDX5 and Other Transcription Factors at the *MYC* Promoter. We have shown that DDX5 is overexpressed in cancer cells (*SI Appendix*, Fig. S4) and enriched at the *MYC* promoter NHE III_1 (Fig. 4*A* and *SI Appendix*, Fig. S5*B*). Moreover, depletion of DDX5 using siRNA can significantly decrease the transcriptional activation of the *MYC* gene in cancer cells (Fig. 4 *C–E* and *SI Appendix*, Figs. S7 and S8). Other transcription factors, including Sp1 (10), hnRNP K (61), and CNBP (11), have been reported to interact with the *MYC* promoter NHE III_1 for *MYC* transcriptional regulation. Tumorigenic MCF7 breast cancer cells were shown to have much higher *MYC* transcription levels as compared to nontransformed MCF10A breast epithelial cells (Fig. 7*A*). We analyzed the enrichment of DDX5 and other transcription factors at the *MYC* promoter in MCF7 and MCF10A cells using ChIP analyses. The ChIP results showed that all of them, including DDX5, are enriched at the *MYC* promoter in MCF7 cells as compared to MCF10A cells (Fig. 7*B*).

Discussion

We have discovered the G4-resolvase activity of DDX5, which actively unfolds the *MYC* promoter DNA G4 structure as well as other intramolecular DNA and RNA G4 structures. DDX5 is one of the founding members of the DEAD-box RNA helicase family (33), whose members have been shown to act only on RNA to date (62). Thus, it was largely unexpected that DDX5 could unfold DNA G4 structures. We showed that DDX5 can recognize the G4 conformation through a structure-based mechanism since DDX5 showed similar binding activity to MycG4(DNA) and MycG4(RNA). Interestingly, we found that the unfolding of G4 by DDX5 occurred in the absence of ATP, whereas addition of ATP did not appreciably alter the unfolding activity. This shows that ATP hydrolysis is not directly coupled to the unfolding process.

We show that the unfolding mechanism of DDX5 is distinct from previously characterized G4 helicases, as DDX5 exhibits active G4-unfolding without requiring a single-stranded tail (as shown in this study). BLM and WRN, members of RecQ family helicases, were the first human helicases reported to resolve G4 DNA in human telomeres (63) and these enzymes function in a 3′→5′ manner (34). The DEAH-box helicase DHX9 and DHX36 (RHAU) were also shown to unfold both RNA and DNA G4 3′→5′ (64–66). Both DHX9 and DHX36 require a 3′ single-stranded region, which is sequence-specific, for loading and G4-unfolding (64–66). All of the reported active G4-helicases are directional/processive and require a single-stranded tail at either the 3′ or 5′ end for loading and G4 unfolding (34). Pot1 and RPA, 2 other proteins associated with G4 destabilization, were found to unfold G4 without a tail (67–69). Pot1 appears to passively trap unfolded ssDNA, while RPA unfolds G4 much faster than a complementary DNA oligonucleotide, implying that RPA has an active mechanism for G4 unfolding. The DEAD-box RNA helicases DDX21, DDX1, and DDX3X were recently reported to unfold or interact with G4s, but only in RNA (70–72). In these cases, the G4-unfolding mechanism is unknown. Thus, DDX5-mediated unfolding represents a description of a G4-unfolding mechanism that is likely direct and also a description of a DEAD-box RNA helicase activity on DNA.

Transcription-associated dynamic negative supercoiling at promoter sites proximal to the *MYC* TSS induces formation of the *MYC* promoter G4. This G4 is a transcription inhibitor by blocking binding of transcriptional activators such as Sp1 (dsDNA) or CNBP and hnRNP K (ssDNA) (8, 25) (Fig. 7*C*). However, the *MYC* G4 structure is thermodynamically very stable under physiologically relevant salt conditions (melting temperature > 85 °C) (28), thus requiring active unfolding in vivo for transcriptional activation. What may facilitate the unfolding has been a missing link. Here, we demonstrated that DDX5 actively unfolds the *MYC* promoter G4 and transactivates the *MYC* oncogene in a G4-dependent manner, defining a mechanism for how this structure

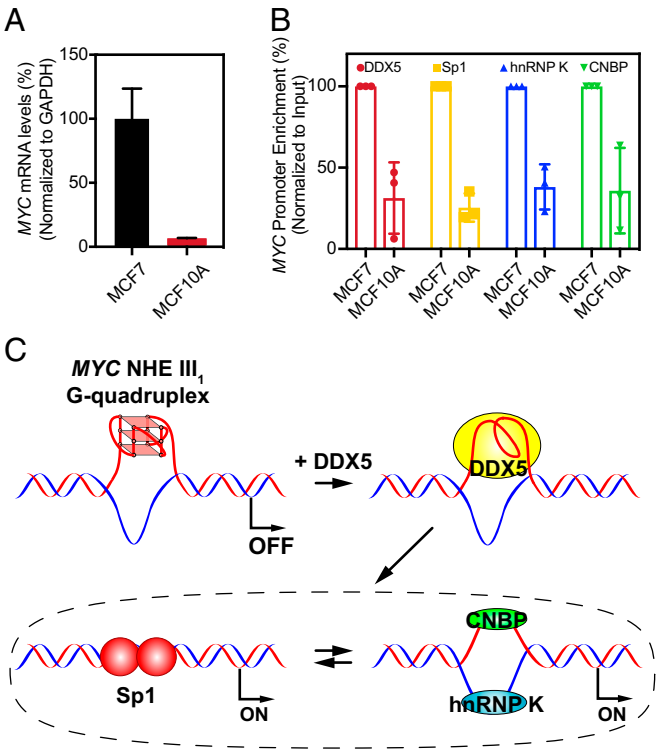

Fig. 7. *MYC* transcriptional regulation via MycG4 in cancer cells. (*A*) The human breast adenocarcinoma cell line MCF7 has a high transcription level of *MYC*, whereas the nontumorigenic human breast epithelial cell line MCF10A has a low *MYC* level. $n = 3$ biologically independent samples. Error bars represent mean ± SEM. (*B*) DDX5, and previously reported transcription factors Sp1, hnRNP K, and CNBP, are more enriched at the *MYC* promoter G4-forming region in the MCF7 cell line compared to MCF10A cell line, suggesting the potential involvement in the active transcription of the *MYC* gene in tumorigenic cells. $n = 3$ biologically independent samples. Error bars represent mean ± SEM. (*C*) A model of transcriptional states associated with the *MYC* promoter G4 and MYC transcriptional regulation by DDX5. The DNA G4 that forms in the *MYC* promoter NHE III_1 region functions as a transcriptional silencer element by preventing the binding of transcription factors (*Upper Left*); DDX5 unfolds the *MYC* promoter G4 (*Upper Right*), likely enabling the binding of transcription factors, such as Sp1 to dsDNA or CNBP and hnRNP K to ssDNA (8, 25), leading to transcriptional activation (*Lower*).

can be resolved in vivo (Fig. 7*C*). It has been shown that within the *MYC* promoter the G4 on the G-rich strand and i-motif secondary structure on the C-rich strand are mutually exclusive (73). Resolution of the stable *MYC* G4 structure by DDX5 may allow the formation of i-motif on the C-rich strand and promote hnRNP K and CNBP binding, or the formation of dsDNA for Sp1 binding, to activate transcription.

Importantly, DDX5 is overexpressed in major human cancers and its overexpression promotes tumorigenesis and tumor progression (36, 37, 39–41, 58). Our results suggest that DDX5 promotes cancer progression through *MYC* transactivation by unfolding of the *MYC* promoter G4. Significantly, we showed that DDX5 interactions with the *MYC* promoter and the DDX5-mediated unfolding of MycG4 can be inhibited by G4-interactive compounds, leading to *MYC* repression and cancer cell death. This result indicates that small molecules targeting the interaction of DDX5 with the *MYC* promoter may be a future strategy for *MYC* down-regulation.

In summary, we discovered DDX5 as a DNA G4 resolvase, elucidated a G4-dependent transactivation mechanism of *MYC* oncogene by DDX5, and established a potential molecular target to down-regulate *MYC* for cancer intervention.

Materials and Methods

Variants of human DDX5 were expressed and purified as described previously (52). Detailed method descriptions of cell viability assay, ChIP-qPCR, CD spectroscopy, DMS footprinting, ELISA, EMSA, fluorescence anisotropy experiments, luciferase assay, qRT-PCR, G4 unfolding assay, and Western blot can be found in *SI Appendix, Supplementary Materials and Methods*.

ACKNOWLEDGMENTS. We thank Drs. Jun Wan and Nadia Lanman for their significant contribution to the bioinformatic analysis; Drs. Kaibo Wang and Clement Lin for their comments; and Clement Lin for proofreading the manuscript. This research was supported by the National Institutes of Health Grants R01CA122952 (to D.Y.), R01CA177585 (to D.Y.), R01GM097332 (to E.J.T.), and P30CA023168 (Purdue Center for Cancer Research), and American Heart Association Predoctoral Fellowship 16PRE31170005 (to Z.X.).

1. J. R. Williamson, M. K. Raghuraman, T. R. Cech, Monovalent cation-induced structure of telomeric DNA: The G-quartet model. *Cell* **59**, 871–880 (1989).
2. W. I. Sundquist, A. Klug, Telomeric DNA dimerizes by formation of guanine tetrads between hairpin loops. *Nature* **342**, 825–829 (1989).
3. D. Yang, K. Okamoto, Structural insights into G-quadruplexes: Towards new anticancer drugs. *Future Med. Chem.* **2**, 619–646 (2010).
4. A. Siddiqui-Jain, C. L. Grand, D. J. Bearss, L. H. Hurley, Direct evidence for a G-quadruplex in a promoter region and its targeting with a small molecule to repress c-MYC transcription. *Proc. Natl. Acad. Sci. U.S.A.* **99**, 11593–11598 (2002).
5. L. T. Gray, A. C. Vallur, J. Eddy, N. Maizels, G quadruplexes are genomewide targets of transcriptional helicases XPB and XPD. *Nat. Chem. Biol.* **10**, 313–318 (2014).
6. M. L. Bochman, K. Paeschke, V. A. Zakian, DNA secondary structures: Stability and function of G-quadruplex structures. *Nat. Rev. Genet.* **13**, 770–780 (2012).
7. R. Rodriguez *et al*., Small-molecule-induced DNA damage identifies alternative DNA structures in human genes. *Nat. Chem. Biol.* **8**, 301–310 (2012).
8. T. A. Brooks, L. H. Hurley, The role of supercoiling in transcriptional control of MYC and its importance in molecular therapeutics. *Nat. Rev. Cancer* **9**, 849–861 (2009).
9. T. Simonsson, P. Pecinka, M. Kubista, DNA tetraplex formation in the control region of c-myc. *Nucleic Acids Res.* **26**, 1167–1172 (1998).
10. E. DesJardins, N. Hay, Repeated CT elements bound by zinc finger proteins control the absolute and relative activities of the two principal human c-myc promoters. *Mol. Cell. Biol.* **13**, 5710–5724 (1993).
11. E. F. Michelotti, T. Tomonaga, H. Krutzsch, D. Levens, Cellular nucleic acid binding protein regulates the CT element of the human c-myc protooncogene. *J. Biol. Chem.* **270**, 9494–9499 (1995).
12. G. Biffi, D. Tannahill, J. McCafferty, S. Balasubramanian, Quantitative visualization of DNA G-quadruplex structures in human cells. *Nat. Chem.* **5**, 182–186 (2013).
13. R. Hänsel-Hertsch *et al*., G-quadruplex structures mark human regulatory chromatin. *Nat. Genet.* **48**, 1267–1272 (2016).
14. I. Wierstra, J. Alves, The c-myc promoter: Still MysterY and challenge. *Adv. Cancer Res.* **99**, 113–333 (2008).
15. K. B. Marcu, A. J. Patel, Y. Yang, Differential regulation of the c-MYC P1 and P2 promoters in the absence of functional tumor suppressors: Implications for mechanisms of deregulated MYC transcription. *Curr. Top. Microbiol. Immunol.* **224**, 47–56 (1997).
16. N. Hay, J. M. Bishop, D. Levens, Regulatory elements that modulate expression of human c-myc. *Genes Dev.* **1**, 659–671 (1987).
17. D. A. T. Sekibo, K. R. Fox, The effects of DNA supercoiling on G-quadruplex formation. *Nucleic Acids Res.* **45**, 12069–12079 (2017).
18. C. Lavelle, Forces and torques in the nucleus: Chromatin under mechanical constraints. *Biochem. Cell Biol.* **87**, 307–322 (2009).
19. F. Kouzine *et al*., Transcription-dependent dynamic supercoiling is a short-range genomic force. *Nat. Struct. Mol. Biol.* **20**, 396–403 (2013).
20. F. Kouzine, S. Sanford, Z. Elisha-Feil, D. Levens, The functional response of upstream DNA to dynamic supercoiling in vivo. *Nat. Struct. Mol. Biol.* **15**, 146–154 (2008).
21. K. W. Zheng *et al*., Superhelicity constrains a localized and R-loop-dependent formation of G-quadruplexes at the upstream region of transcription. *ACS Chem. Biol.* **12**, 2609–2618 (2017).
22. Y. Xia *et al*., Transmission of dynamic supercoiling in linear and multi-way branched DNAs and its regulation revealed by a fluorescent G-quadruplex torsion sensor. *Nucleic Acids Res.* **46**, 7418–7424 (2018).
23. F. Kouzine *et al*., Permanganate/S1 nuclease footprinting reveals non-B DNA structures with regulatory potential across a mammalian genome. *Cell Syst.* **4**, 344–356.e7 (2017).
24. D. Sun, L. H. Hurley, The importance of negative superhelicity in inducing the formation of G-quadruplex and i-motif structures in the c-Myc promoter: Implications for drug targeting and control of gene expression. *J. Med. Chem.* **52**, 2863–2874 (2009).
25. G. A. Michelotti *et al*., Multiple single-stranded cis elements are associated with activated chromatin of the human c-myc gene in vivo. *Mol. Cell. Biol.* **16**, 2656–2669 (1996).
26. Y. Chen, D. Yang, Sequence, stability, and structure of G-quadruplexes and their interactions with drugs. *Curr. Protoc. Nucleic Acid Chem.* **Chapter 17**, Unit17.5 (2012).
27. A. Ambrus, D. Chen, J. Dai, R. A. Jones, D. Yang, Solution structure of the biologically relevant G-quadruplex element in the human c-MYC promoter. Implications for G-quadruplex stabilization. *Biochemistry* **44**, 2048–2058 (2005).
28. E. Hatzakis, K. Okamoto, D. Yang, Thermodynamic stability and folding kinetics of the major G-quadruplex and its loop isomers formed in the nuclease hypersensitive element in the human c-Myc promoter: Effect of loops and flanking segments on the stability of parallel-stranded intramolecular G-quadruplexes. *Biochemistry* **49**, 9152–9160 (2010).
29. J. Seenisamy *et al*., The dynamic character of the G-quadruplex element in the c-MYC promoter and modification by TMPyP4. *J. Am. Chem. Soc.* **126**, 8702–8709 (2004).
30. R. I. Mathad, E. Hatzakis, J. Dai, D. Yang, c-MYC promoter G-quadruplex formed at the 5′-end of NHE III1 element: Insights into biological relevance and parallel-stranded G-quadruplex stability. *Nucleic Acids Res.* **39**, 9023–9033 (2011).
31. P. Linder, E. Jankowsky, From unwinding to clamping—The DEAD box RNA helicase family. *Nat. Rev. Mol. Cell Biol.* **12**, 505–516 (2011).
32. D. P. Lane, W. K. Hoeffler, SV40 large T shares an antigenic determinant with a cellular protein of molecular weight 68,000. *Nature* **288**, 167–170 (1980).
33. H. Hirling, M. Scheffner, T. Restle, H. Stahl, RNA helicase activity associated with the human p68 protein. *Nature* **339**, 562–564 (1989).
34. O. Mendoza, A. Bourdoncle, J. B. Boulé, R. M. Brosh, Jr, J. L. Mergny, G-quadruplexes and helicases. *Nucleic Acids Res.* **44**, 1989–2006 (2016).
35. R. J. Stevenson, S. J. Hamilton, D. E. MacCallum, P. A. Hall, F. V. Fuller-Pace, Expression of the 'dead box' RNA helicase p68 is developmentally and growth regulated and correlates with organ differentiation/maturation in the fetus. *J. Pathol.* **184**, 351–359 (1998).
36. F. V. Fuller-Pace, The DEAD box proteins DDX5 (p68) and DDX17 (p72): Multi-tasking transcriptional regulators. *Biochim. Biophys. Acta* **1829**, 756–763 (2013).
37. L. Yang, C. Lin, Z. R. Liu, Phosphorylations of DEAD box p68 RNA helicase are associated with cancer development and cell proliferation. *Mol. Cancer Res.* **3**, 355–363 (2005).
38. Z. Wang *et al*., DDX5 promotes proliferation and tumorigenesis of non-small-cell lung cancer cells by activating β-catenin signaling pathway. *Cancer Sci.* **106**, 1303–1312 (2015).
39. S. Shin, K. L. Rossow, J. P. Grande, R. Janknecht, Involvement of RNA helicases p68 and p72 in colon cancer. *Cancer Res.* **67**, 7572–7578 (2007).
40. E. L. Clark *et al*., The RNA helicase p68 is a novel androgen receptor coactivator involved in splicing and is overexpressed in prostate cancer. *Cancer Res.* **68**, 7938–7946 (2008).
41. A. Mazurek *et al*., DDX5 regulates DNA replication and is required for cell proliferation in a subset of breast cancer cells. *Cancer Discov.* **2**, 812–825 (2012).
42. R. Janknecht, Multi-talented DEAD-box proteins and potential tumor promoters: p68 RNA helicase (DDX5) and its paralog, p72 RNA helicase (DDX17). *Am. J. Transl. Res.* **2**, 223–234 (2010).
43. F. V. Fuller-Pace, DExD/H box RNA helicases: Multifunctional proteins with important roles in transcriptional regulation. *Nucleic Acids Res.* **34**, 4206–4215 (2006).
44. S. C. Cloutier, W. K. Ma, L. T. Nguyen, E. J. Tran, The DEAD-box RNA helicase Dbp2 connects RNA quality control with repression of aberrant transcription. *J. Biol. Chem.* **287**, 26155–26166 (2012).
45. W. K. Ma *et al*., Recruitment, duplex unwinding and protein-mediated inhibition of the dead-box RNA helicase Dbp2 at actively transcribed chromatin. *J. Mol. Biol.* **428**, 1091–1106 (2016).
46. K. Tago *et al*., Arf tumor suppressor disrupts the oncogenic positive feedback loop including c-Myc and DDX5. *Oncogene* **34**, 314–322 (2015).
47. T. Sengoku, O. Nureki, A. Nakamura, S. Kobayashi, S. Yokoyama, Structural basis for RNA unwinding by the DEAD-box protein Drosophila Vasa. *Cell* **125**, 287–300 (2006).
48. B. G. Kim, H. M. Evans, D. N. Dubins, T. V. Chalikian, Effects of salt on the stability of a G-quadruplex from the human c-MYC promoter. *Biochemistry* **54**, 3420–3430 (2015).

49. L. M. Hellman, M. G. Fried, Electrophoretic mobility shift assay (EMSA) for detecting protein-nucleic acid interactions. *Nat. Protoc.* **2**, 1849–1861 (2007).
50. H. Yao *et al*., Mediation of CTCF transcriptional insulation by DEAD-box RNA-binding protein p68 and steroid receptor RNA activator SRA. *Genes Dev.* **24**, 2543–2555 (2010).
51. P. Machanick, T. L. Bailey, MEME-ChIP: Motif analysis of large DNA datasets. *Bioinformatics* **27**, 1696–1697 (2011).
52. Z. Xing, S. Wang, E. J. Tran, Characterization of the mammalian DEAD-box protein DDX5 reveals functional conservation with *S. cerevisiae* ortholog Dbp2 in transcriptional control and glucose metabolism. *RNA* **23**, 1125–1138 (2017).
53. F. Liu, A. Putnam, E. Jankowsky, ATP hydrolysis is required for DEAD-box protein recycling but not for duplex unwinding. *Proc. Natl. Acad. Sci. U.S.A.* **105**, 20209–20214 (2008).
54. H. Zhang *et al*., RNA helicase DEAD box protein 5 regulates Polycomb repressive complex 2/Hox transcript antisense intergenic RNA function in hepatitis B virus infection and hepatocarcinogenesis. *Hepatology* **64**, 1033–1048 (2016).
55. P. Tijerina, S. Mohr, R. Russell, DMS footprinting of structured RNAs and RNA-protein complexes. *Nat. Protoc.* **2**, 2608–2623 (2007).
56. H. J. Kang, S. Kendrick, S. M. Hecht, L. H. Hurley, The transcriptional complex between the BCL2 i-motif and hnRNP LL is a molecular switch for control of gene expression that can be modulated by small molecules. *J. Am. Chem. Soc.* **136**, 4172–4185 (2014).
57. R. Karaduman, P. Fabrizio, K. Hartmuth, H. Urlaub, R. Lührmann, RNA structure and RNA-protein interactions in purified yeast U6 snRNPs. *J. Mol. Biol.* **356**, 1248–1262 (2006).
58. S. J. Wang, C. Zhang, Y. You, C. M. Shi, Overexpression of RNA helicase p68 protein in cutaneous squamous cell carcinoma. *Clin. Exp. Dermatol.* **37**, 882–888 (2012).
59. C. Shan *et al*., Design, synthesis, and evaluation of isaindigotone derivatives to downregulate c-myc transcription via disrupting the interaction of NM23-H2 with G-quadruplex. *J. Med. Chem.* **60**, 1292–1308 (2017).
60. C. L. Grand *et al*., The cationic porphyrin TMPyP4 down-regulates c-MYC and human telomerase reverse transcriptase expression and inhibits tumor growth in vivo. *Mol. Cancer Ther.* **1**, 565–573 (2002).
61. T. Tomonaga, D. Levens, Activating transcription from single stranded DNA. *Proc. Natl. Acad. Sci. U.S.A.* **93**, 5830–5835 (1996).
62. B. Gilman, P. Tijerina, R. Russell, Distinct RNA-unwinding mechanisms of DEAD-box and DEAH-box RNA helicase proteins in remodeling structured RNAs and RNPs. *Biochem. Soc. Trans.* **45**, 1313–1321 (2017).
63. L. Crabbe, R. E. Verdun, C. I. Haggblom, J. Karlseder, Defective telomere lagging strand synthesis in cells lacking WRN helicase activity. *Science* **306**, 1951–1953 (2004).
64. P. Chakraborty, F. Grosse, Human DHX9 helicase preferentially unwinds RNA-containing displacement loops (R-loops) and G-quadruplexes. *DNA Repair (Amst.)* **10**, 654–665 (2011).
65. M. C. Chen *et al*., Structural basis of G-quadruplex unfolding by the DEAH/RHA helicase DHX36. *Nature* **558**, 465–469 (2018).
66. P. M. Yangyuoru, D. A. Bradburn, Z. Liu, T. S. Xiao, R. Russell, The G-quadruplex (G4) resolvase DHX36 efficiently and specifically disrupts DNA G4s via a translocation-based helicase mechanism. *J. Biol. Chem.* **293**, 1924–1932 (2018).
67. A. J. Zaug, E. R. Podell, T. R. Cech, Human POT1 disrupts telomeric G-quadruplexes allowing telomerase extension in vitro. *Proc. Natl. Acad. Sci. U.S.A.* **102**, 10864–10869 (2005).
68. H. Hwang, N. Buncher, P. L. Opresko, S. Myong, POT1-TPP1 regulates telomeric overhang structural dynamics. *Structure* **20**, 1872–1880 (2012).
69. T. R. Salas *et al*., Human replication protein A unfolds telomeric G-quadruplexes. *Nucleic Acids Res.* **34**, 4857–4865 (2006).
70. E. K. S. McRae *et al*., Human DDX21 binds and unwinds RNA guanine quadruplexes. *Nucleic Acids Res.* **45**, 6656–6668 (2017).
71. C. Ribeiro de Almeida *et al*., RNA helicase DDX1 converts RNA G-quadruplex structures into R-loops to promote IgH class switch recombination. *Mol Cell* **70**, 650–662.e8 (2018).
72. B. Herdy *et al*., Analysis of NRAS RNA G-quadruplex binding proteins reveals DDX3X as a novel interactor of cellular G-quadruplex containing transcripts. *Nucleic Acids Res.* **46**, 11592–11604 (2018).
73. C. Sutherland, Y. Cui, H. Mao, L. H. Hurley, A mechanosensor mechanism controls the G-quadruplex/i-motif molecular switch in the MYC promoter NHE III_1. *J. Am. Chem. Soc.* **138**, 14138–14151 (2016).